

## ARTICLE

## OPEN



# Identifying human body states by using a flexible integrated sensor

Ying Jin<sup>1</sup>, Guoning Chen<sup>2</sup>, Kete Lao<sup>1</sup>, Songhui Li<sup>2</sup>, Yong Lu<sup>1</sup>, Yufeng Gan<sup>1</sup>, Zhundong Li<sup>1</sup>, Jiajia Hu<sup>1</sup>, Jingcheng Huang<sup>1</sup>, Jinxiu Wen<sup>1</sup>, Honggui Deng<sup>1</sup>, Min Yang<sup>2</sup>, Zhiming Chen<sup>1</sup>, Xiaoyan Hu<sup>1</sup>, Baowen Liang<sup>1</sup> and Jianyi Luo<sup>1</sup>✉

Flexible sensors are required to be lightweight, compatible with the skin, sufficiently sensitive, and easily integrated to extract various kinds of body vital signs during continuous healthcare monitoring in daily life. For this, a simple and low-cost flexible temperature and force sensor that uses only two carbon fiber beams as the sensing layer is reported in this work. This simple, flexible sensor can not only monitor skin temperature changes in real time but can also extract most pulse waves, including venous waves, from most parts of the human body. A pulse diagnostic glove containing three such flexible sensors was designed to simulate pulse diagnostic methods used in traditional Chinese medicine. Wearable equipment was also designed in which four flexible sensors were fixed onto different body parts (neck, chest, armpit, and fingertip) to simultaneously monitor body temperature, carotid pulse, fingertip artery pulse, and respiratory rate. Four important physiological indicators—body temperature (BT), blood pressure (BP), heart rate (HR), and respiratory rate (RR)—were extracted by the wearable equipment and analyzed to identify exercise, excited, tired, angry, and frightened body states.

*npj Flexible Electronics* (2020)4:28; <https://doi.org/10.1038/s41528-020-00090-9>

## INTRODUCTION

Real-time monitoring of the state of the human body is very important for human healthcare; however, due to the high costs and inconvenience of the monitoring equipment, monitoring technology is often only applied in the intensive care units of hospitals. If this technology could be extended to wearable equipment that could continuously monitor the health of any patient and even healthy individuals in daily life, early warnings or diagnoses of disease could be obtained for subhealthy people and body states (such as fatigue, excitement, or fear) could be identified by learning the vital data from the bodies of healthy people. The identification of body states could help to remind a tired person to rest and avoid risky behavior, to develop fitness games and other entertainment programs, to assess exercise training intensity, and so on. Recent progress in flexible and wearable electronics has enhanced the possibility of continuous healthcare monitoring in daily life through the development of many kinds of wearable, conformable sensors<sup>1–10</sup>. These sensors mainly include flexible temperature sensors<sup>11–16</sup>, pressure/force sensors<sup>17–25</sup>, humidity sensors<sup>26–29</sup>, ultrasonic sensors<sup>30,31</sup>, optical sensors<sup>32–34</sup>, and biochemical sensors, but most are created to achieve noninvasive detection for a single vital indicator, such as body temperature (BT), heart rate (HR)/arterial pulse, blood pressure (BP), respiratory waves (RWs), or jugular venous pulse. To identify or diagnose human body states, multiple different vital indicators should be monitored continuously. However, the integration of different kinds of sensors into wearable equipment that are compliant with our skin remains challenging.

If one material has multi-sensing property and happens to be a textile fiber, the sensors with different functions could be easily integrated into wearable equipment by using the same sensing material to acquire different vital indicators, just by circuit lead design. In our previous work<sup>35</sup>, the feasibility of the sensor to detect temperature and pressure changes from the outside

environment simultaneously by using only a single carbon fiber beam (CFB) has been demonstrated to be distinguished through the transverse piezo-resistance and longitudinal thermal resistance, respectively. Thus, in this work, a flexible temperature and pressure is easily achieved by fixing only two CFBs of different lengths onto a flexible printed circuit board (FPCB), in which the longer CFB can act as the temperature sensor and the cross-junction of the two CFBs can act as the force sensor. This simple, flexible sensor can not only monitor skin temperature changes in real time but also extract most pulse waves, including venous waves, from most parts of the human body. Four flexible sensors are connected into wearable equipment to simultaneously monitor BT, carotid pulse, fingertip artery pulse, and respiratory rate (RR). Four important physiological indicators, including BT, BP, HR, and RR, are extracted from the body of the subject and are used to identify exercise, excited, tired, angry, and frightened states.

## RESULTS

### Property characterization of the flexible sensor

A flexible sensor for human health monitoring was designed in our work, which integrates pressure/force and temperature sensing on a 1 cm × 1 cm FPCB substrate (Fig. 1a). Two CFBs with different lengths overlap each other to form a cross-junction, to produce an inductive force junction (blue region in Fig. 1a); this cross-junction would sense to the force applied by the tunnel current passing through it. The relatively longer CFB is used to increase the sensitivity of temperature sensing in the temperature area (red region in Fig. 1a). Furthermore, a conductive circuit is provided to allow the pressure and temperature stimulus signals to be distinguished and transmitted without crosstalk by connecting anode 1 or anode 2. The sensor pressure-sensing properties were tested on a three-dimensional mobile control

<sup>1</sup>Research Center of Flexible Sensing Materials and Devices, School of Applied Physics and Materials, Wuyi University, Jiangmen 529020, China. <sup>2</sup>Department of Intelligent Manufacturing, Wuyi University, Jiangmen 529020, China. ✉email: luojiany@mail3.sysu.edu.cn

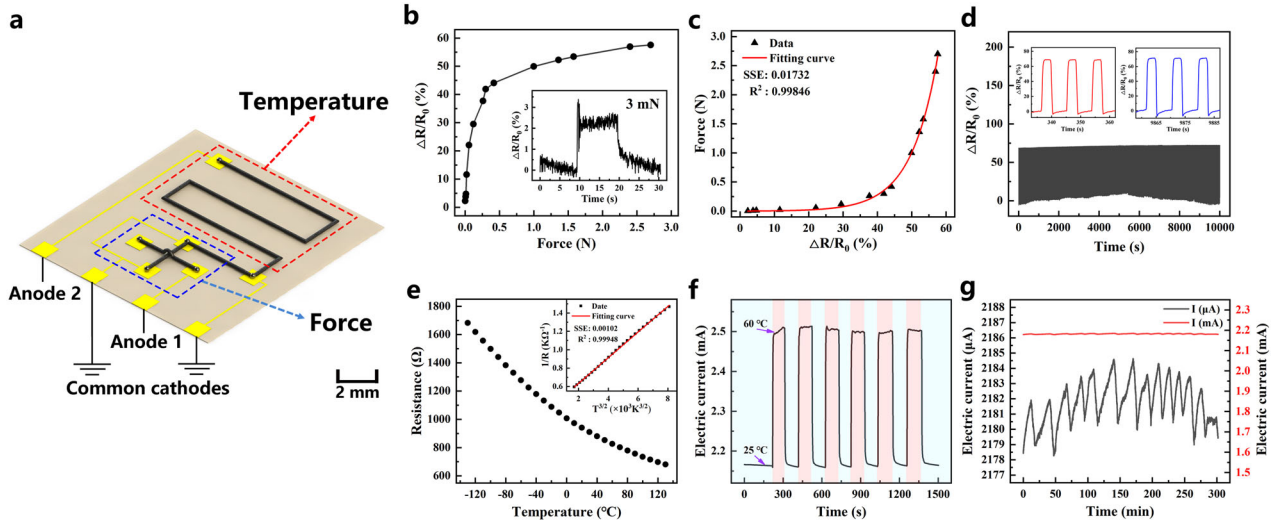


**Fig. 1 Flexible sensor integrated with temperature and force sensing properties.** **a** Schematic diagram for the flexible sensor. **b** Relationship of the resistance change rate with the applied force. Inset: the response curve for the minimum force at 3 mN. **c** Data-fitting curve for the force sensing. **d** A cycling test comprising 1000 cycles under the overload force at 20 N. Inset: the response curves before and after one thousand cycles. **e** Temperature response curve for the flexible sensor. Inset: data-fitting curve satisfying the relationship of the impurity scattering mechanism. **f** Temperature response curves recorded by our flexible sensor during a six heating–cooling cycle test. **g** Five hours temperature stability test at room temperature of 25 °C.

optical platform. As shown in Fig. 1b, a minimum force of 3 mN could be sensed by our sensor, which is sufficiently sensitive for human pulse monitoring. In our previous work, we confirmed that the relationship between the change resistance rate ( $\Delta R/R_0$ ) induced an external force and the compression shift  $\Delta x$ , and it can be written as

$$\frac{|\Delta R|}{R_0} = \frac{R_0(T) - R_0(T)\exp(-k\Delta x)}{R_0(T)} = 1 - \exp(-k\Delta x), \quad (1)$$

where  $k = 1/N\lambda$ ,  $N$  is the number of gaps between two electrodes in the cross-junction, and  $\lambda$  is de Broglie's wavelength for electrons. Thus, the external force size can be characterized by the resistance change rate and the advantage is that the ambient temperature drift when the sensor was used as pressure sensor can be eliminated (for details, see Supplementary Note 1 and Supplementary Fig. 1). Furthermore, we found that the relationship between the resistance change rate and the external force in this flexible sensor can be expressed as

$$F = a(\exp\left(b\frac{|\Delta R|}{R_0}\right) - 1), \quad (2)$$

where  $F$  is the external force, and  $a$  and  $b$  are coefficients determined by data fitting. The data-fitting curve is shown in Fig. 1c. The numerical value of the sum of squared residual error and the goodness of fit ( $R^2$ ) degree indicated that the fitting is very good. Remarkably, this sensor has high sensing stability and good reproducibility under an overloaded force. As shown in Fig. 1d, the test results show that after 1000 cycles under a large overload force of 20 N, the response curve does not indicate worsening behavior from the sensor. Our flexible sensor has high stability even after being struck repeatedly by a hammer (as shown in Supplementary Video 1). This is a highly valuable trait for a wearable sensor, which should be in direct contact with our skin. An extra overload extra force is often carelessly introduced in the wearing process; however, for commercial force sensors, the more sensitive the sensor is, the easier it is to fail under an overload force.

The temperature-sensing properties were tested in the range of ( $-130$  °C and  $130$  °C) on a platform in which the accuracy of the control temperature reached to  $0.1$  °C (Fig. 1e). As the impurities doping occurs frequently during the carbon fibers manufacturing

process, so the longitudinal resistance of CFBs conforms to the impurity scattering mechanism and increases with  $T^{3/2}$ . The longitudinal resistance satisfies this relationship

$$\frac{1}{R} = cT^{\frac{3}{2}} + d, \quad (3)$$

where  $T$  is the temperature in Kelvin, and  $c$  and  $d$  are constant parameters. The data-fitting curve indicates that  $1/R$  (the conductivity of the sensor) increases linearly with  $T^{3/2}$ , which proves that the relationship between the resistance  $R$  and temperature  $T$  in good agreement with the impurity scattering mechanism (for a detailed discussion, see our previous work). Figure 1f shows the temperature response curves during a six heating–cooling cycle test for our flexible sensor. The response current of the sensor is able to return to the initial value after undergoing repeated temperature increases and decreases. The temperature part of our sensor also has excellent stability and sensitivity. The response current of the sensor hardly drifts after 5 h at room temperature, as shown in Fig. 1g. The sensor can even monitor the slight room temperature changes caused by the air conditioner. The fluctuation range is within  $10$  μA.

Here, it should be pointed out that in this sensor, the CFB only needs to meet two conditions, including the structure, which is composed of thousands of fibers with gaps in between, and the impurity doping in each carbon fiber. Most commercial CFBs satisfy these two conditions; thus, among the advantages of the sensor we made is that the materials have been mass-produced and their costs should be lower than those of other nanostructure materials. The maximum sensitivity of the sensor is  $0.66$  kPa<sup>-1</sup> for the pressure part and  $0.32$  °C<sup>-1</sup> for the temperature part. This is in line with the sensitivity levels of pressure and temperature sensors recently reported with nanomaterials (Supplementary Tables 1 and 2, in Supplementary Information).

#### Applications of flexible sensors on the human body

The human circulatory system consists of the heart, blood vessels, and blood. Blood is squeezed into the aorta through the contraction of the heart's left ventricle and then passes to the systemic arteries. Arteries are ducts formed by elastic connective tissue and muscle. When a large amount of blood enters an artery, it increases the pressure inside the vessel and expands its

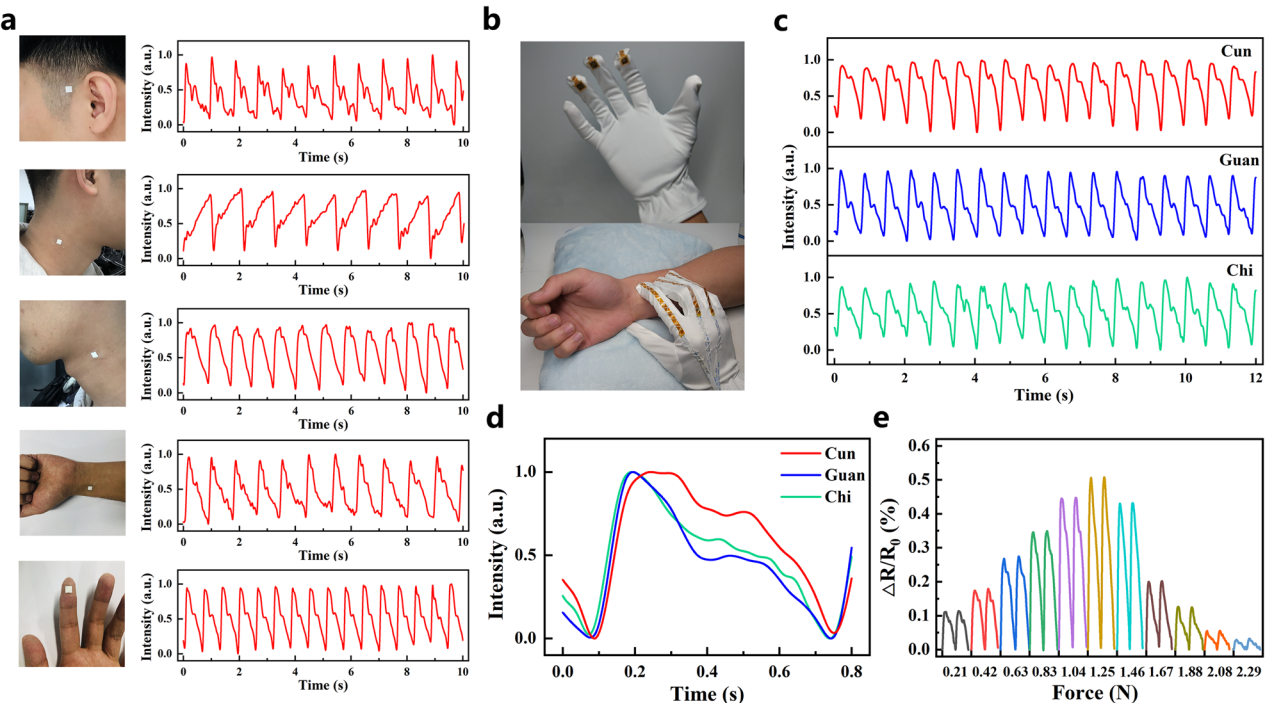


**Fig. 2** Flexible sensors for recording the pulse waves from different acupoints in the body. **a** Typical pulse waves from five acupoints: left superficial temporal artery, right jugular artery, left carotid artery, radial artery, and fingertip artery. **b** A glove equipped with three flexible sensors to simultaneously acquire the pulse wave from three acupoints of traditional Chinese medicine: Cun, Guan, and Chi. **c** Pulse wave from three acupoints of Cun, Guan, and Chi. **d** Comparison of pulse waves within a single period. **e** Pulse waves from Guan acupoint obtained under the different pressure forces.

diameter. We can feel this expansion in in shallow arteries. However, the pulse signal from veins is weaker than the pulse signal from arteries and most commercial sensors cannot sense the venous pulse due to their insufficient sensitivity and large measurement area. The flexible sensor in our work is capable of extracting most of pulse waves, including venous waves, from most parts of the human body due to its high sensitivity and small measurement area for further real-time, noninvasive BP measurements. Figure 2a shows five typical pulse waves from the left superficial temporal artery, right jugular artery, left carotid artery, radial artery, and fingertip artery obtained by placing the device on different human body parts, including the ears, neck, wrists, and fingertips. Pulse is widely used in the field of traditional Chinese medicine (TCM). Diagnoses can be made based on the position, rate, intensity, rhythm, and pattern of the arterial pulse. In TCM syndrome differentiation, pulse as an important basis has important clinical significance for detecting the cause, location, and prognosis of the disease. To visualize TCM diagnosis pulses, we designed a pulse diagnostic glove with a flexible sensor to simulate the pulse diagnosis of TCM (Fig. 2b). Three locations and nine pulse readings have been important signals for TCM pulse diagnostics since ancient times<sup>36,37</sup>. Specifically, this arrangement refers to distinguishing all key characteristics of human organs from the pulse waves at three acupuncture points (Cun, Guan, and Chi) on the radial artery for potential medical diagnosis in the future. The pulse wave patterns from Cun, Guan, and Chi acupoints for a 26-year-old man subject obtained in real time are shown in Fig. 2c. Specifically, the patterns of the different position pulse waves are different for the same subject (Fig. 2d) and the amplitudes of the subject's pulse waves first increase and then decrease with increasing pressure at the same position (Fig. 2e). Static pressure can be applied to each sensor separately, to better imitate the pulse diagnosis technique used in TCM by using this pulse diagnostic glove<sup>38,39</sup>.

BP is an important physiological indicator that reflects the function of blood vessels in the human body, which is of great significance for clinical monitoring and medical diagnosis<sup>40–42</sup>. Unlike traditional BP cuff monitoring, continuous, cuff-less, and noninvasive BP monitoring performed by measuring the pulse wave velocity (PWV) can provide the time resolution required to detect BP fluctuations caused by exercise or mood fluctuations, and is considered an effective and reproducible method for measuring BP. The PWV can be calculated via the Moens-Korteweg equation<sup>43,44</sup>

$$PWV = \sqrt{\frac{Eh}{2\rho r}}, \quad (4)$$

where  $E$  and  $h$  are the elastic modulus and the thickness of the vessel wall, respectively,  $r$  and  $\rho$  are the radius of the artery and the density of the blood, respectively. Some experiments showed that the BP scales with  $PWV^2$ , i.e.,  $BP \approx aPWV^2$ , where  $a$  depends on the properties of the artery. For the same subject, the condition of the blood vessels will not change much in a period of time and so the scaling coefficient  $a$  is approximately constant. Accordingly, the relation between BP and PWV can be represented by<sup>45,46</sup>

$$BP = aPWV^2 + \beta, \quad (5)$$

where  $a$  and  $\beta$  are the undetermined coefficients whose values vary with each individual.

Two identical sensor devices were worn on the left index finger and left ear to collect pulse waves, so as to demonstrate the capability of the flexible sensor system to perform real-time BP measurement. The two sensor devices were connected to an NI 9234 acquisition card and the acquired signals were then displayed in real time and saved to a personal computer through data acquisition software. As the acquisition rate of the NI 9234 is 5120 times  $s^{-1}$ , the signals from the equipment can be strictly synchronized for pulse transmit time (PTT) and BP calculations.

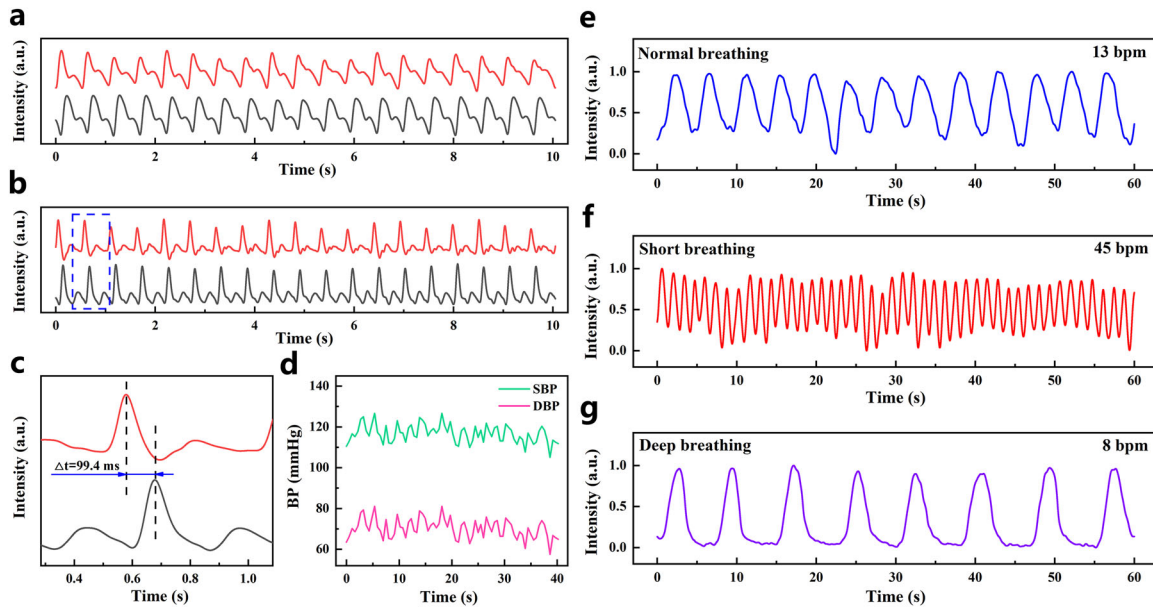


**Fig. 3 Flexible sensors for detecting blood pressures and respiratory waves in real time.** **a** Pulse waves from left carotid artery (red) and Index fingertip artery (black). **b** Differential conversion curves of the ones in **a**. **c** Enlarged curves for the region marked by a blue virtual box in **b** showing the pulse transmit time is 99.4 ms. **d** Systolic blood pressure (SBP) and diastolic blood pressure (DBP) curve obtained in real time by the pulse transmit time. **e–g** Breathing waves at normal breathing, short breathing, and deep breathing states by a flexible sensor fixed on the chest.

The data of pulse waveforms are presented in Fig. 3a. Here we perform first-order differentiation of the obtained data to effectively reduce the error in calculating the PTT (Fig. 3b). This calculation yielded a 99.4 ms time delay between the signal acquired from the left fingertip and that from the left ear (Fig. 3c). Here, the PWV can be calculated by

$$\text{PWV} = \frac{d}{\text{PTT}}, \quad (6)$$

where  $d$  is the transmission distance of the pulse wave. Then, BP can be calculated by

$$\text{BP} = a \frac{d^2}{\text{PTT}^2} + \beta. \quad (7)$$

The transmission distance of the pulse wave does not change for the same individual. Consequently, BP can be calculated by

$$\text{BP} = \frac{A}{\text{PTT}^2} + B, \quad (8)$$

where  $A$  and  $B$  are undetermined coefficients whose values vary from individual to individual.

During the measurement, the BP was intermittently measured with a cuff BP monitor (OMRON T31). Ten different BP data points were selected and fitted according to the formula to obtain the BP formula of the subject and the real-time BP curve, as shown in Fig. 3d. Similarly, RR is another important physiological indicator. Because of the high sensitivity of the flexible sensors, we provide a convenient method for monitoring the RR. The expansion and contraction of the chest cavity induces a press and release process in a flexible sensor attached to a subject's chest in one breathing cycle. Figure 3e–g shows three different breathing states (normal, short, and deep breathing), with RRs of 13, 45, and 8 b.p.m., respectively.

Furthermore, this flexible sensor could be easily installed in wearable electronic equipment in the future to monitor the human body and skin temperature in real time. To observe the temperature response of the flexible sensor, we attached the sensor to the palm of the subject. As a comparison, we recorded the palm temperature of the subject with a commercial infrared

camera at the same time (Fig. 4a). Before the experiment, the air conditioner was turned on to adjust the indoor temperature of the laboratory to a constant temperature of 17 °C, the subject remained seated in a relaxed state at room temperature of (26 °C) for 20 min and then entered the laboratory to start the experiment. During the entire experiment, the subject was seated in a chair wearing an ordinary T-shirt and his left palm was flat on a table and remained stationary. As shown in Fig. 4b, the temperature response curve of our sensor had the same trend as the temperature curve of the commercial infrared camera during the test, which proves that the flexible sensor has excellent performance in monitoring human skin temperature. When entering a high- or low-temperature environment, the human body will automatically adjust the surface temperature to adapt to the drastic changes in the ambient temperature. Interestingly, we observed that the skin temperature continued to decrease in a periodic rather than a linear manner until the skin temperature was constant.

#### Identifying human body states

BT, BP, HR, and RR are all important physiological indicators of the human body. We aimed to collect these four physiological indicator changes when the human body switched between different states by using wearable equipment with four flexible sensors as an exploration of the possibility of identifying body states with these vital signs in the future. Figure 5a shows the wearable equipment, in which four flexible sensors were fixed onto the different body parts (neck, chest, armpit, and fingertip), and the Bluetooth acquisition board, measuring 45 mm × 15 mm, including the analog-to-digital converter, Wheatstone bridge, and Bluetooth module (Supplementary Note 2 and Supplementary Fig. 2 in Supplementary Information). Four vital sign changes for the exercise, tired, excited, and angry states are shown in Fig. 5b–e. We discovered that the BT increased in the exercise and the excited states increased and decreased in the tired and angry states, respectively; the BP increased in the excited and angry states, decreased in the tired state, and was almost unchanged in the exercise state; the HR increased significantly in the exercise,

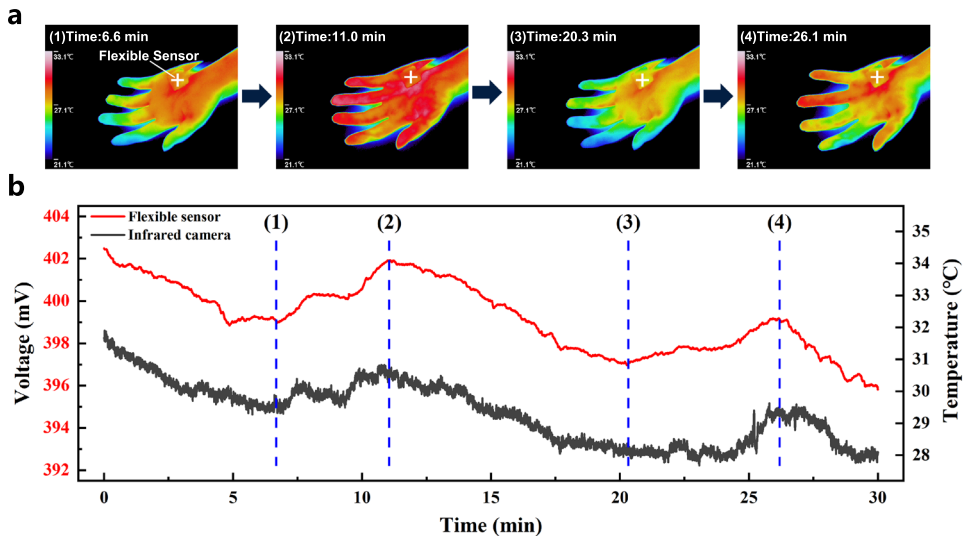


**Fig. 4 Flexible sensors for monitoring the skin temperature change.** **a** Infrared images for the skin temperature change process on the palm in an air-condition room at 17 °C. **b** Temperature response curves for the skin temperature change recorded by the flexible sensor (red) and the infrared camera (black), respectively.

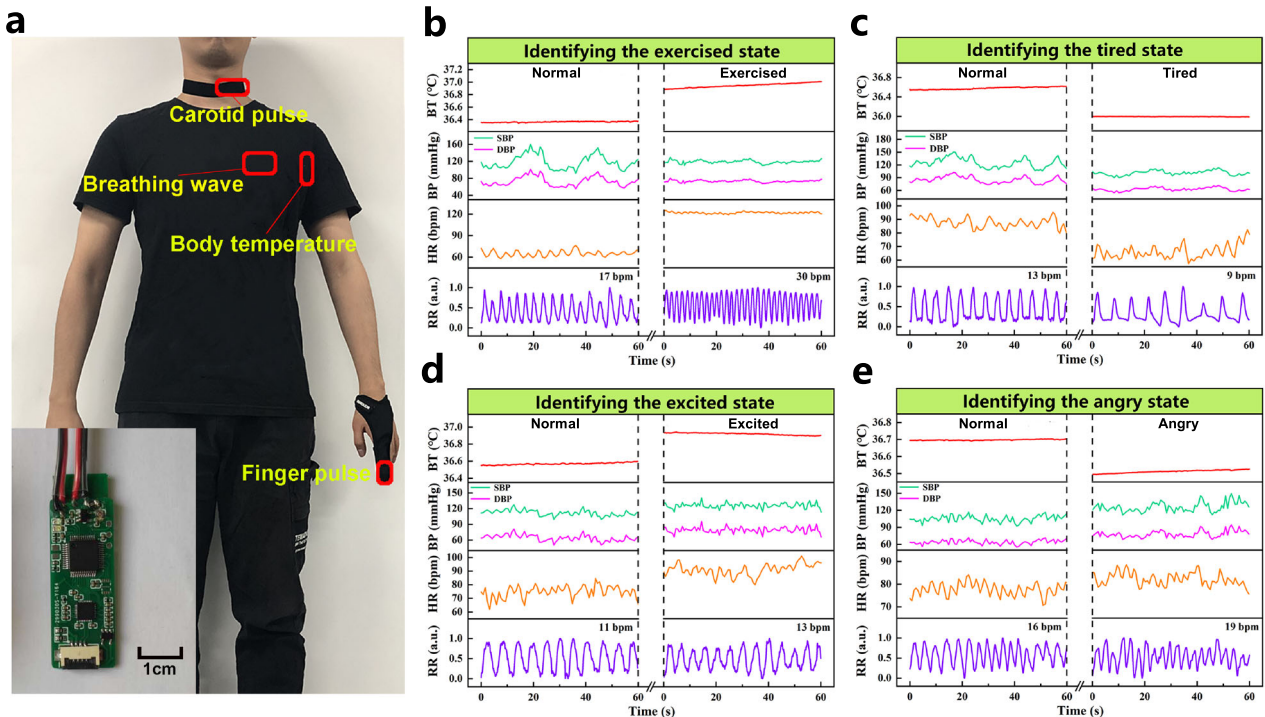


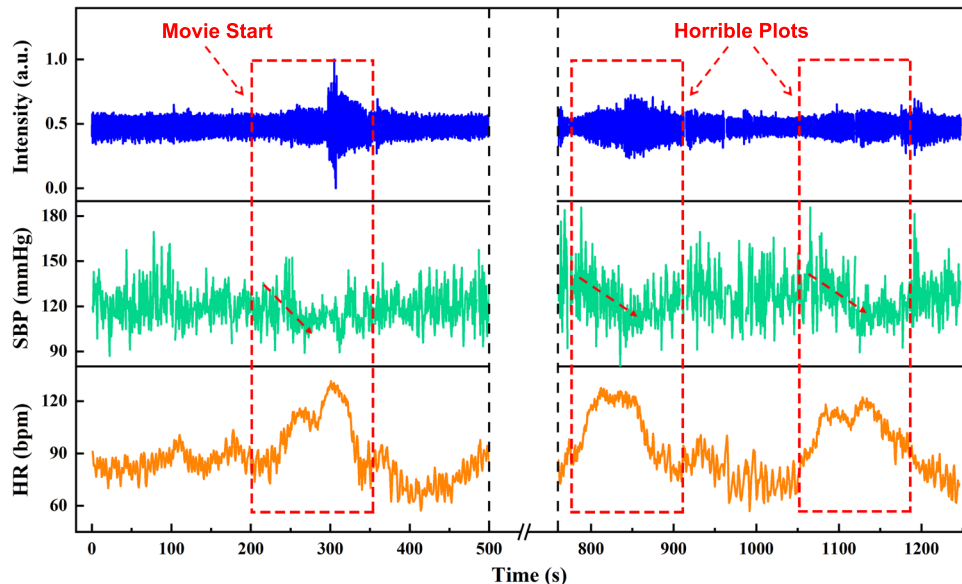
**Fig. 5 Identification of the human body states.** **a** Photograph of the wearable equipment in which four flexible sensors are used to simultaneously acquire four vital signs from the tester: body temperature (BT), blood pressure (BP), heart rate (HR), and respiratory rate (RR). Inset: the Bluetooth acquisition board. **b–e** Four vital signs change for the exercise, tired, excited and angry states, respectively.

excited, and angry states and decreased in the tired state; and the RR increased in the exercise, excited, and angry states and decreased in the tired state. The data from the four physiological indicators under the different body states are summarized and listed in Table 1. First, the degree of distinction for the tired state was greatest, indicating that these four indicators were decreasing when the subject was getting tired. Second, the degree of distinction was lower for the exercise and excited states; most of the indicators increased, although the BP measured by our wearable equipment was obviously unchanged. However, it should be noted that the BP measured by the wearable

equipment was significantly different from the BP measured by the commercial BP monitoring in the exercise state, but the trend was the same for the other states. The reasons for this need to be explored. Thus, based on these results, the exercise state is best distinguished from the other states by the HR and RR, as the HR and RR increased significantly in the exercise state but only slightly in the excited and angry states. The only difference between the excited and angry states is in the BT indicator, which slightly increased in the excited state, while decreasing in the angry state. Accordingly, we may be able to identify the body state even if the subject is not aware of it (e.g., fatigued/tired

**Table 1.** Listing on the changes of four human vital signs under the different body states.

States	Exercised	Tired	Excited	Angry
Indexes				
BT (°C)	↑ (+0.5 °C)	↓ (-0.5 °C)	↑ (+0.4 °C)	↓ (-0.2 °C)
BP (mmHg)	Unchanged	↓ (-20 mmHg)	↑ (+10 mmHg)	↑ (+10 mmHg)
HR (b.p.m.)	↑ (+55 b.p.m.)	↓ (-25 b.p.m.)	↑ (+20 b.p.m.)	↑ (+7 b.p.m.)
RR (b.p.m.)	↑ (+13 b.p.m.)	↓ (-4 b.p.m.)	↑ (+2 b.p.m.)	↑ (+3 b.p.m.)

**Fig. 6 Capturing transient state of startle.** The transient state is captured by continuously monitoring the carotid artery wave (up curve), blood pressure (middle curve), and heart rate (down curve) when the tester is scared by a movie.

driving) in the future by learning and analyzing sufficient data from these vital signs.

Finally, we captured the changes in physiological indicators caused by horror scenes in a movie (Fig. 6) by using our wearable equipment. When the movie started, the subject showed excitement, i.e., the pulse intensity of the carotid artery was enhanced, and the HR obviously increased. After ~150 s, the excitement induced at the start of the movie disappeared and the HR returned to normal. Then, when the subject encountered horror footage, the pulse intensity of the carotid artery and the HR suddenly increased, whereas the BP dropped rapidly. The change in body state caused by the startled shock lasted for ~100 s and gradually returned to normal. In particular, although the BP value returned to a relatively stable state soon after receiving the shock, the average BP value gradually increased over time and the BP curve fluctuated more severely. Although these changes were successfully collected by our wearable equipment, the relationship between these changes and the regulation of the human body needs to be investigated by biological researchers.

## DISCUSSION

In summary, a simple and low-cost flexible sensor was fabricated by fixing only two crossed CFBs on an FPCB substrate, in which the cross-junction of the CFBs is ultrasensitive to weak force changes, whereas the longitudinal resistance of one of CFBs is highly sensitive to temperature changes. Thus, when the flexible sensor is applied in healthcare monitoring, it can be used as a force sensor to detect HR and as a flexible temperature sensor to detect BT changes by merely switching the connecting anodes according

to the monitoring requirements. In terms of force sensing, the flexible sensor was demonstrated to be able to extract most pulse waves, including those from the carotid artery, radial artery, fingertip artery, and veins, from most parts of the human body. One specific application of the flexible sensors, a pulse diagnostic glove, was designed to simulate the pulse diagnostic methods of TCM. In terms of temperature sensing, the flexible sensor can be easily installed into wearable electronic equipment to monitor human BT in real time and has outstanding performance in capturing the automatic adjustment of BT in response to drastic changes in the ambient temperature. By using this flexible sensor, BT, BP, HR, and RR could be extracted simultaneously by the wearable equipment and applied to monitor the exercise, excited, tired, angry, and frightened states of the human body, and to establish a connection between changes in these physiological indicators and the human body states. This work indicates the feasibility of identifying human body states by using flexible sensors to noninvasively monitor its vital signs.

## METHODS

### Fabrication of the flexible sensors

The flexible sensor mainly included a sensing layer and a polyimide (PI) protecting film. The sensing layer included a substrate using 1 cm × 1 cm FPCB, six surface mounted device (SMD) pads, copper-clad conductive circuit, and two CFBs. The CFBs were placed on the substrate as shown in the Fig. 1a, then the CFBs were fixed on the substrate by applying conductive adhesive to the six SMD pads. Then, the PI film was covered narrowly on the sensing layer to form a flexible sensor.

### Pressure-sensing test

The pressure-sensing test was characterized by a commercial force gauge (M7-10, Mark-10) and a z-axis translation stage (EM303, Mark-10). In the force-sensitivity test, the force gauge was controlled to squeeze the pressure sensor and the resistance of sensor was recorded in different force from 0 to 2.7 N. In the cycling test, the sensor was subjected to 1000 cycles under the overload force at 20 N.

### Temperature-sensing test

Characteristic tests of carbon fiber temperature Sensor were obtained using heating and freezing stage system (Linkam HFS600E-PB4). The electrical signals at both ends of carbon fiber were tested by two tungsten microprobes with the temperature varying from  $-130$  to  $130$  °C. The heating-cooling cycle test was achieved by switching the sensor between in the hot (60 °C) and room temperature (25 °C) water, and the steady supply voltage was fixed at 1.0 V and the current change was monitored by a source meter (Keithley 2450).

### Human pulse, RW, and BP test

Before the experiment, the subject was kept in sitting posture in a relaxed state for 20 min and then the sensors were fixed on the measured position to start the test. During the entire experiment, the subject was sitting in a chair. Further, in RW test, the sensor was attached to the left upper chest position. In the BP test, the sensor was fixed to the left carotid artery and the left index fingertip, and a commercial wrist electronic BP monitor (OMRON T31) was worn before the experiment, the wrist was raised to the same height as the heart, and the fingers were flat. During the experiment, the BP was intermittently measured with the BP monitor. The two sensor devices were connected to the NI 9234 acquisition card and then the acquired signals can be displayed in real time and saved in a personal computer through soft programming. As the acquisition rate of the NI 9234 is 5120 times  $s^{-1}$ , the signals from the two sensors can be strictly synchronized for accurate PTT and BP calculations. The two-channel pulse data and corresponding BP values of the same subject were measured in multiple groups. Then, the data of ten different BP values were selected and fitted to obtain the subject's BP formula.

### Palm-temperature test

Before the experiment, the indoor temperature of the laboratory was adjusted to a constant temperature of 17 °C by using an air conditioner; the subject was kept in sitting posture in a relaxed state in another room at 26 °C for 20 min. The subject entered the laboratory, the sensor was fixed to the left palm position, and then turned on the infrared camera (AVIO, R550Pro) to start the test. During the entire experiment, the subject was sitting on a chair, wearing an ordinary T-shirt, his left palm was flat on the table, and remained stationary.

### Four body status test

Before the experiment, the subject was kept in a sitting posture in a relaxed state for 20 min. The devices were worn as shown in Fig. 5a, to start the test. The data were recorded in the normal state.

In exercised state test, the subject moved to the sports ground, ran for 35 min, and did fast leg lift for 5 min. The total exercise time was 40 min. The data were recorded as exercised state in time after the exercise. In tired status test, the subject's normal state test time was 8:50 in the morning and the tired-state test time was 8:50 the next day. There was no rest for 24 h and the subject was confirmed to be in a fatigue state. In excited status test, the subject played a 1 h online competitive game, then the subject achieved consecutive victories and confirmed to be in an excited state by asking. Data were collected in time after the game and were recorded as exercised state. Unlike the excited state test, in the angry state test, the subject achieved consecutive failures and confirmed to be in an angry state by asking.

### Startle transient test

Before the experiment, the subject was kept in sitting posture in a relaxed state for 20 min. The devices were worn as shown in Fig. 5a and the subject sat in front of the computer to start the test. Started playing horror movie after collecting data for a period of time. Throughout the experiment, the wrist was raised to the same height as the heart and the fingers were flat. The experiments involving human subjects have been performed with the

full, informed consent of the volunteers, who are also co-authors (first, third, and fifth authors) of the manuscript.

### Image-processing details

All data about human body with the flexible sensor were processed using Butterworth filtering. The data of infrared camera were not processed.

## DATA AVAILABILITY

The experimental data referenced in this text is available from the authors upon reasonable request.

Received: 27 April 2020; Accepted: 26 August 2020;

Published online: 16 October 2020

## REFERENCES

1. Gao, W. et al. Fully integrated wearable sensor arrays for multiplexed in situ perspiration analysis. *Nature* **529**, 509–514 (2016).
2. Gao, Y., Yu, L., Yeo, J. C. & Lim, C. T. Flexible hybrid sensors for health monitoring: materials and mechanisms to render wearability. *Adv. Mater.* **32**, e1902133 (2020).
3. Yao, S., Swetha, P. & Zhu, Y. Nanomaterial-enabled wearable sensors for health-care. *Adv. Healthc. Mater.* **7**, 1700889 (2018).
4. Wan, Y., Wang, Y. & Guo, C. F. Recent progresses on flexible tactile sensors. *Mater. Today Phys.* **1**, 61–73 (2017).
5. Dias, D. & Paulo Silva Cunha, J. Wearable health devices-vital sign monitoring, systems and technologies. *Sensors* **18**, 2414 (2018).
6. Liu, Y. et al. Flexible, stretchable sensors for wearable health monitoring: sensing mechanisms, materials, fabrication strategies and features. *Sensors* **18**, 645 (2018).
7. Wang, Z., Zhang, L., Liu, J. & Li, C. A flexible bimodal sensor based on an electrospun nanofibrous structure for simultaneous pressure-temperature detection. *Nanoscale* **11**, 14242–14249 (2019).
8. An, B. W., Heo, S., Ji, S., Bien, F. & Park, J. Transparent and flexible fingerprint sensor array with multiplexed detection of tactile pressure and skin temperature. *Nat. Commun.* **9**, 2458 (2018).
9. Wu, R. et al. Silk composite electronic textile sensor for high space precision 2D combo temperature-pressure sensing. *Small* **15**, e1901558 (2019).
10. Zhao, S. & Zhu, R. Flexible bimodal sensor for simultaneous and independent perceiving of pressure and temperature stimuli. *Adv. Mater. Technol.* **2**, 1700183 (2017).
11. Hong, S. Y. et al. Stretchable active matrix temperature sensor array of polyaniline nanofibers for electronic skin. *Adv. Mater.* **28**, 930–935 (2016).
12. Zeng, X. et al. Silver telluride nanowire assembly for high-performance flexible thermoelectric film and its application in self-powered temperature sensor. *Adv. Electron. Mater.* **5**, 1800612 (2019).
13. Jung, M. et al. Paper-based bimodal sensor for electronic skin applications. *ACS Appl. Mater. Inter.* **9**, 26974–26982 (2017).
14. Yamamoto, Y. et al. Efficient skin temperature sensor and stable gel-less sticky ECG sensor for a wearable flexible healthcare patch. *Adv. Healthc. Mater.* **6**, 1700495 (2017).
15. Trung, T. Q. et al. A stretchable strain-insensitive temperature sensor based on free-standing elastomeric composite fibers for on-body monitoring of skin temperature. *ACS Appl. Mater. Inter.* **11**, 2317–2327 (2019).
16. Liu, Q. et al. A high-performances flexible temperature sensor composed of polyethyleneimine/reduced graphene oxide bilayer for real-time monitoring. *Adv. Mater. Technol.* **4**, 1800594 (2019).
17. Guo, Y., Zhong, M., Fang, Z., Wan, P. & Yu, G. A wearable transient pressure sensor made with MXene nanosheets for sensitive broad-range human-machine interfacing. *Nano Lett.* **19**, 1143–1150 (2019).
18. Schwartz, G. et al. Flexible polymer transistors with high pressure sensitivity for application in electronic skin and health monitoring. *Nat. Commun.* **4**, 1859 (2013).
19. Yamamoto, Y. et al. Printed multifunctional flexible device with an integrated motion sensor for health care monitoring. *Sci. Adv.* **2**, e1601473 (2016).
20. Liu, M. et al. Large-area all-textile pressure sensors for monitoring human motion and physiological signals. *Adv. Mater.* **29**, 1703700 (2017).
21. Hua, Q. et al. Skin-inspired highly stretchable and conformable matrix networks for multifunctional sensing. *Nat. Commun.* **9**, 244 (2018).
22. Xi, W., Yeo, J. C., Yu, L., Zhang, S. & Lim, C. T. Ultrathin and wearable microtubular epidermal sensor for real-time physiological pulse monitoring. *Adv. Mater. Technol.* **2**, 1700016 (2017).
23. Wang, Y. et al. Wearable and highly sensitive graphene strain sensors for human motion monitoring. *Adv. Funct. Mater.* **24**, 4666–4670 (2014).
24. Pang, C. et al. Highly skin-conformal microhairy sensor for pulse signal amplification. *Adv. Mater.* **27**, 634–640 (2015).

25. Ma, Y. et al. 3D synergistical MXene/reduced graphene oxide aerogel for a piezoresistive sensor. *ACS Nano* **12**, 3209–3216 (2018).
26. Li, T. et al. Porous ionic membrane based flexible humidity sensor and its multifunctional applications. *Adv. Sci.* **4**, 1600404 (2017).
27. Ma, L. et al. Full-textile wireless flexible humidity sensor for human physiological monitoring. *Adv. Funct. Mater.* **29**, 1904549 (2019).
28. Wei, Z. et al. Flexible nanowire cluster as a wearable colorimetric humidity sensor. *Small* **13**, 1700109 (2017).
29. Wang, Y., Zhang, L., Zhou, J. & Lu, A. Flexible and transparent cellulose-based ionic film as a humidity sensor. *ACS Appl. Mater. Inter.* **12**, 7631–7638 (2020).
30. Jiang, L. et al. Flexible piezoelectric ultrasonic energy harvester array for bio-implantable wireless generator. *Nano Energy* **56**, 216–224 (2019).
31. Wang, C. et al. Monitoring of the central blood pressure waveform via a conformal ultrasonic device. *Nat. Biomed. Eng.* **2**, 687–695 (2018).
32. Haseda, Y. et al. Measurement of pulse wave signals and blood pressure by a plastic optical fiber FBG sensor. *Sensors* **19**, 5088 (2019).
33. Payne, R. A., Symeonides, C. N., Webb, D. J. & Maxwell, S. R. J. Pulse transit time measured from the ECG: an unreliable marker of beat-to-beat blood pressure. *J. Appl. Physiol.* **100**, 136–141 (2006).
34. Park, S. et al. Self-powered ultra-flexible electronics via nano-grating-patterned organic photovoltaics. *Nature* **561**, 516–521 (2018).
35. Huang, J. et al. Flexible integrated sensors: transverse piezoresistance and longitudinal thermal resistance of one single carbon fiber beam. *Adv. Mater. Technol.* **4**, 1900802 (2019).
36. Chu, Y. et al. Human pulse diagnosis for medical assessments using a wearable piezoelectret sensing system. *Adv. Funct. Mater.* **28**, 1803413 (2018).
37. Lin, D. et al. Detection of multipoint pulse waves and dynamic 3D pulse shape of the radial artery based on binocular vision theory. *Comput. Meth. Prog. Bio.* **155**, 61–73 (2018).
38. Xue, Y. et al. Full-field wrist pulse signal acquisition and analysis by 3D digital image correlation. *Opt. Laser Eng.* **98**, 76–82 (2017).
39. Chung, Y., Hu, C., Yeh, C. & Luo, C. How to standardize the pulse-taking method of traditional Chinese medicine pulse diagnosis. *Comput. Biol. Med.* **43**, 342–349 (2013).
40. Boutry, C. M. et al. A sensitive and biodegradable pressure sensor array for cardiovascular monitoring. *Adv. Mater.* **27**, 6954–6961 (2015).
41. Fan, X. et al. Alignment-free liquid-capsule pressure sensor for cardiovascular monitoring. *Adv. Funct. Mater.* **28**, 1805045 (2018).
42. Luo, N. et al. Flexible piezoresistive sensor patch enabling ultralow power cuffless blood pressure measurement. *Adv. Funct. Mater.* **26**, 1178–1187 (2016).
43. Meng, K. et al. Flexible weaving constructed self-powered pressure sensor enabling continuous diagnosis of cardiovascular disease and measurement of cuffless blood pressure. *Adv. Funct. Mater.* **29**, 1806388 (2019).
44. Bramwell, C. J. & Hill, A. V. The velocity of the pulse wave in man. *Proc. R. Soc. B* **93**, 298–306 (1922).
45. Ma, Y. et al. Relation between blood pressure and pulse wave velocity for human arteries. *Proc. Natl. Acad. Sci. USA* **115**, 11144–11149 (2018).
46. Thomas, S. S. et al. BioWatch: a non-invasive wrist-based blood pressure monitor that incorporates training techniques for posture and subject variability. *IEEE J. Biomed. Health* **20**, 1291 (2016).

## ACKNOWLEDGEMENTS

The major work was carried out in School of Applied Physics and Materials, and Research Center of Flexible Sensing Materials and Devices in Wuyi University. It is

mainly supported by Guangdong Natural Science foundation for Distinguished Young Scholar (2015A030306031), National Natural Science Foundation of China (51802229), Natural Science Foundation of Guangdong Province (2018A030313561), and Innovation and strong school engineering fund of Guangdong Province (2016KQNCX169 and 2017KTSCX186). This work is also supported in part by the Science and Technology Projects of Jiangmen ((2017) 307, (2017) 149, and (2018) 352), Cooperative education platform of Guangdong Province ((2016) 31), Key Laboratory of Optoelectronic materials and Applications in Guangdong Higher Education (2017KSYS011), and Science Foundation for Young Teachers of Wuyi University (2018td04).

## AUTHOR CONTRIBUTIONS

All authors contributed to the preparation of this paper. J.L. and Y.J. conceived the research idea. They co-wrote the manuscript with contributions from all authors. J.L., J.W., M.J., and Z.C. supervised the overall project. Y.J., J.H., X.H., and B.L. helped in the realization of sensor. G.C. and Y.G. helped in the realization of electronics. S.L., Z.L., and J.H. helped in the realization of graphical user interface. Experimental data were taken by Y.J., K.L., Y.L., and H.D.

## COMPETING INTERESTS

The authors declare no competing interests.

## ADDITIONAL INFORMATION

**Supplementary information** is available for this paper at <https://doi.org/10.1038/s41528-020-00090-9>.

**Correspondence** and requests for materials should be addressed to J.L.

**Reprints and permission information** is available at <http://www.nature.com/reprints>

**Publisher's note** Springer Nature remains neutral with regard to jurisdictional claims in published maps and institutional affiliations.



**Open Access** This article is licensed under a Creative Commons Attribution 4.0 International License, which permits use, sharing, adaptation, distribution and reproduction in any medium or format, as long as you give appropriate credit to the original author(s) and the source, provide a link to the Creative Commons license, and indicate if changes were made. The images or other third party material in this article are included in the article's Creative Commons license, unless indicated otherwise in a credit line to the material. If material is not included in the article's Creative Commons license and your intended use is not permitted by statutory regulation or exceeds the permitted use, you will need to obtain permission directly from the copyright holder. To view a copy of this license, visit <http://creativecommons.org/licenses/by/4.0/>.

© The Author(s) 2020